Augmented-plane-wave calculation and measurements of K and L x-ray spectra for solid Ni

Frank Szmulowicz and Douglas M. Pease
Institute of Materials Science, University of Connecticut, Storrs, Connecticut 06268
(Received 9 September 1977; revised manuscript received 6 December 1977)

X-ray absorption and emission K and L spectra for solid Ni were calculated using the band structure and wave functions obtained from our augmented-plane-wave program. High spectral resolution and accuracy were achieved by a careful treatment of the Ni potential, band structure, wave functions, dipole matrix elements, $\vec{k}$-space integrations and interpolations, and broadening due to core level widths; however, core-hole many-electron effects on the final-state wave functions were not included. Measurements of nickel K and L absorption-edge spectra were carried out using a two-crystal spectrometer, and the resulting spectra were corrected for instrumental window effects. The experimental and theoretical absorption spectra show excellent overall agreement with respect to positions and strengths of corresponding structures although, at threshold, the experimental K edge is somewhat rounded and the experimental L edge enhanced, relative to the corresponding theoretical spectra. For the case of the emission spectra, the calculated L spectrum is considerably broader than would be indicated by most of the experimental x-ray valence-band results.

I. INTRODUCTION

Absorption and emission spectra provide a method for probing many aspects of the unoccupied and occupied states, respectively, or materials: the selection rules for x-ray processes allow an investigation of separate angular momentum components of the total density of states. The experimental x-ray spectra provide rich structure typically over a 20–30-eV range which yields information for semiempirical adjustment of potentials used in band calculations, as in the scheme of Chen and Segall.[1] Comparison of theoretical band-structure calculations with experiment provides an additional method for testing the limits of validity of one-electron calculations for both ground- and excited-state properties of solids; such comparisons can be used to evaluate the contribution of many-body effects to the spectra so as to facilitate the testing of many-body theories.

While emission spectra have been the subject of many calculations, there has not been a corresponding effort in the calculation of absorption spectra. The few systems that have been studied include Al by Szmulowicz and Segall,[2] Mg, Na, Li by Gupta and Freeman,[3] and Ca,[4] Ni,[5] TiFe,[6] V,[7] NbC,[7] TiNi,[7] and V_3Si,[7] by Papaconstantopoulos and coworkers. Whereas the nearly-free-electron absorption spectra of Mg, Na, and Li were calculated out to a few eV above threshold in order to exhibit one-electron effects upon the spectra, we are interested in testing predictions of band calculations over a larger energy range in a transition metal having unfilled $3d$ states.

For Ni metal, there has been one previous calculation of the x-ray absorption spectra.[5] Our calculation represents an improvement over that of Nagel *et al.* in the following ways: we identify structure in the spectrum and have a higher spectral resolution. We have included no adjustable hot-electron broadening corrections in our calculation. Although such corrections are undoubtedly important for the highly excited states above the Fermi level, we obtain generally good experimental-theoretical agreement using core-hole broadening alone. Brillouin-zone sums are done in our work using a very accurate Gilat and Raubenheimer (GR) method[8] whereas Nagel *et al.* use a Monte Carlo technique with 2000 points in the zone. Finally, and perhaps most important to the accuracy, is the interpolation technique. We use a universally applicable $\vec{k}\cdot\vec{p}$ scheme instead of relying on a QUAD polynomial interpolation method.

Enumerating other details of the calculation, we note that we used the result of our augmented-plane-wave (APW) program for paramagnetic Ni. The $3d^{9.4}4s^{0.6}$ configuration was used as in the calculations by Stocks, Williams, and Faulkner.[9] Energy bands and wave functions were obtained at 89 $\vec{k}$ points in the Brillouin zone, in a 4-Ry range above the conduction-band minimum, and each state was decomposed into its angular components. Matrix elements of the momentum operator between all states in the 4-Ry range and between $1s$, $2p$ and conduction states were computed using the APW wave functions. The bands and other relevant quantities were interpolated to a 3123 GR mesh using the $\vec{k}\cdot\vec{p}$ method and $\vec{k}$-space integrations were done using the GR method which is relatively noiseless as compared to the Monte Carlo technique. The absorption spectra are given in absolute units allowing the testing of oscillator-strength computations by comparing the magnitude of the calculated spectra with experiments. We finally compared the theoretical calculations with K and L absorption-

edge measurements performed on the same two-crystal spectrometer with appropriate corrections made for instrumental distortions.

In Sec. II, the results of the APW calculation for bands, wave functions, partial charge densities, and oscillator strengths are given. Section III contains the discussion of $\vec{k}$-space integration and interpolation methods used in this calculation as well as general comments about computations of the density of states, Fermi energy, linear absorption coefficient, emission spectra, and partial charge densities. In Sec. IV the computed spectra are presented and analyzed; structures in the spectra are assigned to various symmetry levels. Spectrum broadening is discussed in Sec. V and experimental methods are presented in Sec. VI. Core-level broadened computed spectra are compared with experiments in Sec. VII and are followed by our conclusions.

II. BAND STRUCTURE

The band structure of Ni has been calculated by several authors.[5,10-22] Except for the calculation by Nagel *et al.* all others were done in the energy range up to about the Fermi level. The ferromagnetic Ni calculations of Connolly (APW),[15] Callaway and co-workers (GTO)[19-22] were done using the "spin-polarized" method. The very extensive treatment of Callaway and co-workers included self-consistent iteration of the band structure,[20,22] adjustment of the exchange coefficient α,[19,20] inclusion of the spin-orbit coupling[21] and calculations of the Fermi surface cross sections,[19-22] density of states,[19-22] charge and spin densities,[20,22] contact charge densities,[22] spin and charge density form factors,[20,22] and the magneton number.[19-22] Additionally, Williams, Janak and Maruzzi,[23] and Wang and Callaway[21] have computed the optical spectrum for the paramagnetic and ferromagnetic Ni, respectively.

In our calculation we used the symmetrized version of the APW method (SAPW) to solve the secular equation at 89 $\vec{k}$ points in the irreducible wedge of the Brillouin zone in a 4-Ry range above the muffin-tin zero. In constructing the secular equation, the l summation, corresponding to the spherical harmonics expansion of the wave function inside the muffin-tin radius in spherical harmonics, was carried up to $l_{\max}=10$. The variational expansion of the total wave function in terms of augmented plane waves included reciprocal-lattice wave vectors $\vec{K}_i$, up to $|\vec{k}_i|=\vec{k}+\vec{K}_i$ such that $|\vec{k}_i|r_m < 7.42$, where r_m is the muffin-tin radius. The above limits determine the convergence of the eigenvalues and, according to the rules developed by Switendick, are supposed to produce d bands converged to within 0.001 Ry.[24]

We used the Ni potential that was constructed by Stocks, Williams, and Faulkner for their work on NiCu alloys.[9] Stocks *et al.* constructed the potential from the atomic Ni charge densities that were obtained from a slightly modified version of the Herman and Skillman[25] program (no Latter cutoff plus logarithmic radial mesh) using a $3d^{9.4}4s^{0.6}$ atomic configuration for Ni. This configuration was proposed for the theoretical study of paramagnetic Ni for comparison with experiments performed on ferromagnetic Ni. This atomic structure was designed to simulate the occupation of electronic levels in the ferromagnetic phase of Ni. As x-ray emission and absorption spectra are rather insensitive to the small exchange splitting of the conduction bands, the above configuration represents a reasonable approximation to the real system. The Ni crystal potential was then constructed by a superposition of the atomic charge densities according to the prescription of Mattheiss.[26]

Figure 1 displays the energy versus wave-vector plots for Ni, in a 4-Ry range, along important symmetry directions. Our energy eigenvalues agree with the corresponding eigenvalues of the KKR calculation of Stocks *et al.* to within 0.001 Ry. The energy-band plot, Fig. 1, exhibits the familiar narrow d bands and the hybridization with s-p bands. The Fermi level is at $E_F=0.678$ Ry, resulting in some empty d bands such as the X_5 and W_1' levels. Note the existence of rather flat bands above E_F which will figure in the subsequent analysis of structure in the density of states and the K and L absorption of Ni. Most important of these are $\Delta_2'(\Gamma_2'\rightarrow X_3)$ whose character goes from f-like at Γ_2' to d-like at X_3, $Z_1[X_1(s,d)\rightarrow W_2'(p,d)]$, $Q_1[W_3(p,d)\rightarrow L_1(s,d)]$, and $Q_1[W_3(p,d)\rightarrow L_3(d)]$. Another feature of the bands relevant to the analysis of the frequency spectra is the occurrence of minima and maxima of bands along symmetry lines. These arise primarily as a consequence of the interaction of bands belonging to the same irreducible representation of the point group of the wave vectors on the symmetry axes, and due to hybridization. An inspection of Fig. 1 reveals that several such minima and maxima occur along the symmetry lines of fcc Ni. Additionally, we have identified several band extrema on symmetry planes of the Brillouin zone.

It is interesting to note that the energy bands of Ni above the $3d$ region exhibit qualitative features characteristic of s,p bands (here $4s,4p$) of the nearly-free-electron metals like Al($3s^23p^1$). And apart from some modifications due to level reorderings, different band gaps, the Fermi-level position, and band widths, the band structure of nick-

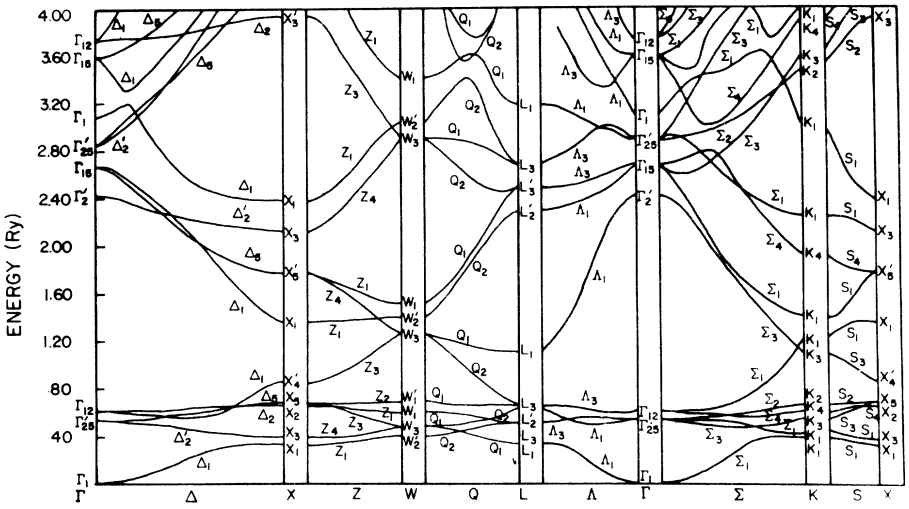

FIG. 1. Paramagnetic Ni band structure in 4-Ry range along symmetry directions ($a = 6.6321$ a.u., $V_c = -1.1329$ Ry, $E_F = 0.678$ Ry).

el and that for copper[27,28] are very similar in the extended energy range.

The normalized wave functions of Ni for all 89 $\vec{k}$ points and for all the bands were solved by a back substitution into the secular equation. The l character of each eigenstate was obtained by calculating the lth component of the eigenstate's normalization q_l for the part of the wave function inside the muffin-tin radius

$$1 = \sum_l q_l + Q_{\text{out}} , \tag{1}$$

where Q_{out} is the portion of the wave function's "charge" contained in the interstitial part of the unit cell.

The q_l values give directly the degree of localization of each wave function inside the muffin-tin region, and Q_{out} the charge which is contained in the plane-wave part of the total wave function in the interstitial region. The Q_{out} values should be compared with the fraction of the unit cell's volume outside the muffin-tin region, which is 0.26 for the fcc unit cell in the touching muffin-tin sphere configuration.

Results of our calculation reveal that the d states Γ'_{25}, Γ_{12}, X_3, X_2, X_5, L_1, L_3, W'_2, W_3, W_1, W'_1, K_1, K_3, K_4, and K_2 have their "d charge" (i.e., the portion of the normalization contained in the $l = 2$ component of the wave function) very well localized inside the muffin-tin sphere (around 90%). Therefore, the atomic description of the $3d$ bands is well justified. Higher-energy states have their charge contained in the interstitial region more in proportion to the fraction of the total volume in that part of the unit cell. This validates the nearly-free-electron treatment of these bands and points to the utility of using an orthogonalized-plane-wave (OPW) description of the bands of $3d$ metals when combined with a tight-binding treatment of the $3d$ bands.

It is clear that the high-energy states acquire progressively larger components of high l character. In this calculation the wave functions were calculated by retaining terms up to $l_{\max} = 10$ in order to reflect this fact. Keeping such large l values is crucial to the accuracy of the subsequent evaluation of the x-ray spectra and for an evaluation of interband matrix elements of the momentum operator (MEM) that are needed for the $\vec{k}\cdot\vec{p}$ interpolation.

The MEM's between all the bands at 89 $\vec{k}$ points in the fcc irreducible wedge were calculated by a straightforward application of the momentum operator to the wave functions. We did not use any operator identities for MEM evaluation because they do not permit one to obtain, in a straightforward manner, the energy gradients. In addition, some identities such as the $\vec{\nabla}V(\vec{r})$ method $(\vec{P}_{mn}(\vec{k}) = (1/i)\{\langle \vec{k}m|\vec{\nabla}V(\vec{r})|\vec{k}n\rangle/[E_m(\vec{k}) - E_n(\vec{k})]\})$, suffer from convergence problems for closely spaced bands.[2]

The $K(1s)$ and $L(2p)$ core-level wave functions were obtained from the solution of the radial Schrödinger equation using the Ni crystal potential. (Spin-orbit splitting was not included for the $2p$ states.) The program used to obtain the conduction-band radial wave functions was used here as well. The core wave functions were assumed to be of the form

$$\Psi_{nlm}(\vec{r}) = R_{nl}(r) Y_l^m(\hat{r}) , \tag{2}$$

where the R's are the normalized radial wave functions and the Y's are the appropriate spherical harmonics. The R's calculated with our program were very well localized inside r_m and were in

TABLE I. Core to conduction band $|\mathrm{MEM}|^2$ at symmetry points in Ni (in Ry).

	K	L		K	L		K	L
Γ_1	0.0000	1.3148×10^{-1}	L_1	0.0	2.8249	K_1	2.0085×10^{-2}	3.4729
Γ'_{25}	0.0000	4.9152	L_3	0.0	4.8343	K_1	4.1135×10^{-2}	3.7541
Γ_{12}	0.0000	5.4281	L'_2	4.8527×10^{-1}	0.0	K_3	9.1955×10^{-2}	4.1207
Γ'_2	0.0000	0.0000	L_3	0.0	5.7622	K_4	5.5712×10^{-3}	5.3915
Γ_{15}	4.5337×10^{-1}	0.0000	L_1	0.0	3.1628	K_2	0.0	5.7293
Γ'_{25}	0.0000	2.6138	L'_2	4.0568×10^{-2}	0.0	K_3	4.3618×10^{-1}	1.8007
Γ_1	0.0000	1.3712×10^{-2}	L'_3	7.5748×10^{-1}	0.0	K_1	3.2664×10^{-1}	2.0075
Γ_{15}	9.2924×10^{-1}	0.0000	L_3	0.0	2.4401	K_1	2.4442×10^{-3}	1.9839
Γ_{12}	0.0000	2.5302	L_1	0.0	1.3097	K_4	5.7080×10^{-1}	4.7345×10^{-1}
						K_1	2.9112×10^{-2}	1.6552
X_1	0.0	3.1312	W'_2	4.0259×10^{-2}	3.4776	K_1	3.0667×10^{-1}	8.8956×10^{-1}
X_3	0.0	3.9677	W_3	5.9857×10^{-2}	3.9918	K_2	0.0	7.9113×10^{-1}
X_2	0.0	5.6737	W_1	0.0	5.0534	K_3	1.1487×10^{-1}	3.3695×10^{-1}
X_5	0.0	5.8548	W'_1	0.0	5.8574	K_4	4.6278×10^{-1}	1.3210
X'_4	5.5643×10^{-1}	0.0	W_3	4.5019×10^{-1}	1.6651	K_1	8.7252×10^{-2}	7.5357×10^{-1}
X_1	0.0	2.9682	W'_2	2.2576×10^{-1}	2.7185			
X'_5	6.0025×10^{-1}	0.0	W_1	0.0	7.1889×10^{-1}			
X_3	0.0	3.2140	W_3	9.2015×10^{-2}	1.1433			
X_1	0.0	8.4173×10^{-1}	W'_2	7.3334×10^{-1}	2.1474×10^{-1}			
X'_3	0.0	0.0	W_1	0.0	1.3690			

very good agreement with the corresponding R's calculated for Ni by Herman and Skillman.[25] The form chosen for the core-level wave functions assumes the levels to be dispersionless, i.e., $E(\vec{k})$ = const.

The MEM's which are proportional to "oscillator strengths," for core to conduction-band transitions were calculated for all the bands at 89 $\vec{k}$ points. In Table I the $|\mathrm{MEM}|^2$ for these interband transitions are listed; for the $2p$ levels the sum of the $|\mathrm{MEM}|^2$ for all three $m=-1,0,1$ sublevels is given.

It is clear that the entries in Table I give just another measure of the magnitude of the various l components of the conduction-band wave functions. The K and L columns are proportional to the transition probabilities for core to conduction-band excitations. An examination of the table reveals that the transition probabilities are much stronger for the L spectra than for the K. Additionally, the MEM's for the $3d$ bands appear to be nearly constant irrespective of their Brillouin-zone (BZ) symmetry, again pointing to their atomic character. The MEM's are quite strongly wave-vector and energy dependent ruling out a common constant MEM approximation.

III. $\vec{k}$-SPACE INTEGRATION AND INTERPOLATION

The $\vec{k}\cdot\vec{p}$ scheme was used to interpolate the energy bands, the MEM's, and the $q_l(\vec{k})$'s from the 89-point mesh of the APW calculation to a grid of 3128 points in the irreducible wedge (i.e., 32 cube subdivision of the Δ axis). The $\vec{k}\cdot\vec{p}$ scheme has an advantage over other methods of interpolation in that it is generally applicable to all metals, regardless of the energy range covered. In contrast to polynomial schemes, the $\vec{k}\cdot\vec{p}$ method is capable of producing a faithful representation of band crossings, thus eliminating a source of spurious structures in frequency spectra. The $\vec{k}\cdot\vec{p}$ secular determinants were solved with a very accurate Jacobi diagonalization procedure, using all the bands available at the original APW grid. The Jacobi eigenvalue-eigenvector method, unlike many other schemes, produces N orthonormal eigenfunctions at an N-fold degenerate root. Specific details of the $\vec{k}\cdot\vec{p}$ interpolation are given in Ref. 2.

The following $\vec{k}$-space integrals were evaluated for paramagnetic nickel using the GR scheme.

(i) Density of states [electrons/(atom Ry)] for energy ω,

$$D(\omega)=\frac{2\Omega}{(2\pi)^3}\sum_n\int d^3k\,\delta(\omega-E(\vec{k},n)) =\frac{2\Omega}{(2\pi)^3}\sum_n\sum_{\vec{k}_0}\frac{\Delta S_\omega}{|\vec{\nabla}_{\vec{k}}E(\vec{k},n)|_0}\,, \tag{3}$$

where the volume integral on the right-hand side has been replaced by a surface integral in the discrete sum over small cubes centered at $\vec{k}_0$, and ΔS_ω is an element of a constant ω energy surface in a cube, Ω is the unit-cell volume, and n is a band index.

(ii) Integrated density of states (electrons/atom)

$$N(\omega)=\int_0^\omega D(\omega')\,d\omega'=\frac{2\Omega}{(2\pi)^3}\int_{E(\vec{k},n)\le\omega}d^3k\,, \tag{4}$$

which was performed with a variant of the GR

scheme for volume elements (relevant formulas are given in Ref. 2).

(iii) Angular momentum decomposed partial-charge densities

$$Q_l(\omega) = \sum_n \int d^3k\, q_l(\vec{k},n)\delta(\omega - E(\vec{k},n)) , \tag{5}$$

where $q_l(\vec{k},n)$ is the lth component of the total charge contained in $\Psi(\vec{k},n)$—the wave function for band n at wave vector $\vec{k}$, so that

$$\langle\Psi(\vec{k},n)|\Psi(\vec{k},n)\rangle = 1 = \sum_l q_l(\vec{k},n) + Q_{\text{out}}(\vec{k},n) .$$

(iv) Linear absorption coefficient for the K and L x-ray absorption in the dipole approximation for cubic materials

$$\mu(\omega) = \frac{\omega\epsilon_2(\omega)}{nc}$$

$$= \frac{8}{3nc\omega\pi} \sum_m \int d^3k\, |\vec{P}_{jm}(\vec{k})|^2 \delta(\omega - E(\vec{k},m) + E_j) , \tag{6}$$

where $n \simeq 1$ is the real part of the complex index of refraction $N = n + i\kappa$, κ is the extinction coefficient, ϵ_2 is the imaginary part of the dielectric constant, c is the speed of light, j denotes the appropriate core level, and $|\vec{P}_{jm}(\vec{k})|^2$ is the core to band m $|\text{MEM}|^2$. In the above, atomic units are used.

The GR scheme is very suitable for the evaluation of the above integrals. In this method the irreducible wedge is filled with a large number of cubes, although fewer than for the Monte Carlo method. Once energies and their gradients at the cube centers are known, the GR procedure, by making a linear energy expansion, approximates constant energy surfaces by planes. The $\vec{k}$-space integration is then reduced to the surface integration by virtue of the δ function in 3, 5, and 6, with area elements ΔS_ω given analytically. Placing the cube centers $\vec{k}_0$ at an offset mesh avoids singular points in the integrals where the energy gradients vanish for reasons of symmetry. Since a rather small number of cubes is required for a good convergence of the $\vec{k}$ sums, the use of the accurate but time-consuming $\vec{k}\cdot\vec{p}$ interpolation becomes economically feasible.

IV. PRESENTATION OF UNBROADENED SPECTRA

The density of states for Ni is shown in Fig. 2. The curve was calculated on a 0.005-Ry mesh and, thus, has a high spectral resolution. The arrows on the graph point to the locations of structure in the curve and are labeled by the irreducible representation of the symmetry point which is the source of the structure. For structures caused by band extrema at a point on a symmetry line, the location of the point on the line is given in parentheses in units of $2\pi/8a$, i.e., x, y, z, and similarly for points on symmetry planes. Horizontal arrows over the spectrum indicate the energy ranges spanned by symmetry lines which by virtue of being flat lead to a large magnitude of the density in the corresponding energy range. Also, note the similarity between the Cu density of states computed by Janak, Williams, and Moruzzi[28] and that for Ni, Fig. 2.

The analysis of structure in Fig. 2 is important for several reasons. First, it summarizes experimentally observable properties not immediately

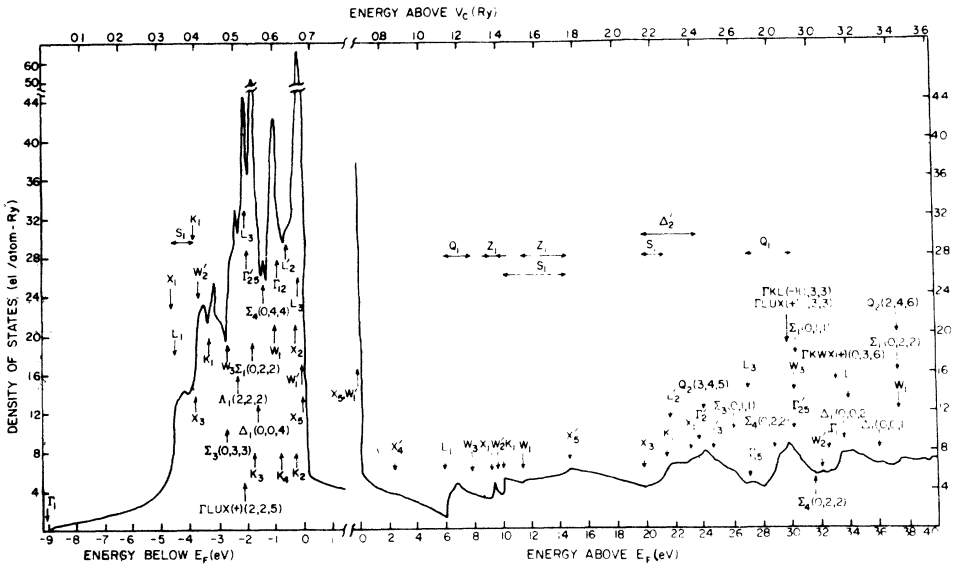

FIG. 2. Density of states for Ni. Structure in the spectrum is indicated by the arrows and is labeled by irreducible representation and its location is given in units of $2\pi/8a$.

TABLE II. List of energy levels which contribute to the structure in the density of states. The list contains the band's irreducible representation, indices, energy, l character, and Q_{out}. For bands on symmetry lines and planes, the location of the singular point is given in parentheses in units of $2\pi/8a$. Energies are given with respect to the Fermi level in eV.

Level	Band(s)	Energy (eV)	q_s	q_p	q_d	Q_{out}
Γ_1	1	−9.037	0.7009	0.0	0.0	0.2990
X_1	1	−4.618	0.0555	0.0	0.8012	0.1429
L_1	1	−4.525	0.1760	0.0	0.7090	0.1142
K_1	1	−3.854	0.0221	0.0271	0.8227	0.1235
X_3	2	−3.813	0.0	0.0	0.9372	0.0619
W_2'	1	−3.700	0.0	0.0543	0.8121	0.1292
K_1	2	−3.393	0.0083	0.0592	0.8499	0.0809
W_3	2,3	−2.682	0.0	0.0799	0.8447	0.0703
$\Sigma_3(0,3,3)$	2	−2.630	0.0	0.0291	0.9155	0.0486
$\Lambda_1(2,2,2)$	2	−2.376	0.0076	0.0506	0.8750	0.0594
$\Gamma LUX(+)(2,2,5)$	3	−2.129	0.0276	0.0432	0.8689	0.0532
L_3	2,3	−2.070	0.0	0.0	0.9682	0.0278
Γ_{25}'	2,3,4	−1.973	0.0	0.0	0.9761	0.0198
$\Sigma_1(0,2,2)$	3	−1.775	0.0003	0.0079	0.9622	0.0241
K_3	3	−1.718	0.0	0.1214	0.8007	0.0712
$\Delta_1(0,0,4)$	3	−1.581	0.0447	0.0351	0.8626	0.0489
$\Sigma_4(0,4,4)$	4	−1.395	0.0	0.0047	0.9658	0.0234
W_1	4	−1.010	0.0163	0.0	0.9537	0.0218
Γ_{12}	5,6	−0.930	0.0	0.0	0.9904	0.0071
K_4	4	−0.773	0.0	0.0728	0.9722	0.0156
L_2'	4	−0.582	0.0	0.6326	0.0	0.3544
K_2	5	−0.210	0.0	0.0	0.9927	0.0039
X_2	3	−0.202	0.0	0.0	0.9960	0.0032
L_3	5,6	−0.157	0.0	0.0	0.9949	0.0037
X_5	4,5	0.051	0.0	0.0	0.9970	0.0020
W_1'	5	0.059	0.0	0.0	0.9970	0.0020
X_4'	6	2.449	0.0	0.6982	0.0	0.2734
K_3	6	5.856	0.0	0.5213	0.2590	0.2042
L_1	7	6.044	0.4412	0.0	0.4384	0.1185
K_1	7	7.265	0.0612	0.3819	0.2905	0.2391
W_3	6,7	7.847	0.0	0.5216	0.2456	0.2099
X_1	7	9.276	0.3446	0.0	0.4379	0.2150
W_2'	8	9.704	0.0	0.2537	0.4203	0.3090
K_1	8	10.073	0.4716	0.0027	0.2883	0.1937
W_1	9	11.389	0.6807	0.0	0.0834	0.1390
X_5'	8,9	14.710	0.0	0.6173	0.0	0.2245
X_3	10	19.889	0.0	0.0	0.7117	0.2739
K_1	10	21.511	0.1683	0.0262	0.3698	0.2974
L_2'	8	21.769	0.0	0.0362	0.0	0.4940
X_1	11	23.150	0.4991	0.0	0.1554	0.2778
Γ_2'	7	23.845	0.0	0.0	0.0	0.4112
$Q_2(3,4,5)$	10	24.101	0.0	0.4468	0.0117	0.2480
L_3'	9,10	24.678	0.0	0.6392	0.0	0.1347
$\Sigma_3(0,1,1)$	9	26.114	0.0	0.2793	0.0310	0.3163
Γ_{15}	8,9,10	27.173	0.0	0.3631	0.0	0.3020
L_3	11,12	27.191	0.0	0.0	0.6464	0.2907
$\Sigma_4(0,2,2)$	11	28.967	0.0	0.0558	0.2951	0.3487
$\Gamma LUX(+)(1,1,3)$	11	29.452	0.0931	0.6136	0.1479	0.1457
$\Gamma KL(-)(1,3,3)$	11	29.597	0.0	0.2321	0.3877	0.2172
Γ_{25}'	11,12,13	30.293	0.0	0.0	0.7376	0.1972
W_3	10,11	30.355	0.0	0.0689	0.3230	0.2751
$\Sigma_1(0,1,1)$	11	30.388	0.0111	0.0461	0.3417	0.3626
$\Sigma_4(0,2,2)$	13	31.667	0.0	0.7559	0.1113	0.0740
W_2'	12	32.175	0.0	0.5282	0.0622	0.2655
Γ_1	14	32.687	0.0785	0.0	0.0	0.6683
$\Gamma KWX(+)(0,3,6)$	12	33.291	0.1397	0.0245	0.3877	0.2581
$\Delta_1(0,0,2)$	14	33.696	0.0598	0.6314	0.1445	0.0974

TABLE II. (*Continued*)

Level	Bands(s)	Energy (eV)	q_s	q_p	q_d	Q_{out}
L_1	13	34.083	0.2583	0.0	0.3608	0.2497
$\Delta_1(0,0,1)$	15	36.665	0.0422	0.2707	0.2849	0.2144
W_1	13	37.418	0.2389	0.0	0.3753	0.2382
$\Sigma_1(0,2,2)$	14	37.459	0.1179	0.1250	0.5191	0.1701
$Q_2(2,4,6)$	12	37.481	0.0	0.0305	0.2709	0.2910

obtainable from the energy plots, and it identifies the energy levels in the BZ responsible for maxima and minima in the spectra. In addition, the position of structures monitors changes in electronic properties in response to modifications introduced by alloying, stresses, etc.

The information contained in Fig. 2 is summarized in Table II where band indices, energy, Q_{out}, and l-charge decomposition for all the levels are given. Figures 3–5 give the decomposition of the total charge into s, p, and d contributions, respectively. These curves are labeled in the same way as the density-of-states curve, Fig. 2, except that, of course, the labels pertain to states having the appropriate l character. By referring to the energy-band plot, Fig. 1, and to Table II, it is straightforward to locate the bands with zero gradients and, therefore, the structure in the curves. Of course, additional energy-band plots, not shown here, and the computer printout were used to locate band extremas on symmetry planes.

The computed K and L x-ray spectra of Ni are shown in Figs. 6 and 7, respectively, following the notations of Fig. 2. Aside from one weak structure, the K emission is rather simple, consisting of one large peak. The magnitude of K emission is due largely to the s-p,d hybridization, e.g., note the second Δ_1 band which turns over at $(2\pi/8a)$ (0, 0, 4) and the second Λ_1 band which has a minimum along Λ at $(2\pi/8a)$ (2, 2, 2). On the other hand, the K absorption spectrum exhibits a number of pronounced maxima at X_4', X_5'; $Q_2(3,4,5)$ and L_3'; $\Gamma KL(-)(1,3,3)$ and $\Gamma LUX(+)(1,1,3)$; W_2'; $\Delta_1(0,0,2)$; and $\Sigma_1(0,2,2)$; from Table II these levels can be seen to be strongly p-like. An interesting plateau at about 7 eV is caused by a large number of p states in that energy region. Additionally, some of the minima in the K spectrum occur at energies of strongly s,d-like levels $L_1(s,d)$, $X_3(d)$, $K_1(s,d)$, and $L_3(d)$.

From Figs. 3 and 5 it is apparent that the L spectrum is dominated by the d components of the conduction states. The X_5 and W_1' d levels are above E_F and account for the large magnitude of the L absorption at the threshold. The L emission spectrum exhibits a large number of narrow peaks caused by correspondingly narrow d bands of Ni. When the core-level broadening is taken into account only the two largest peaks will be seen. There is a sharp onset of transitions from the L shell at L_1, and the two structures at 10 eV are due to X_1, W_2', K_1, and an extremely flat Z_1 band.

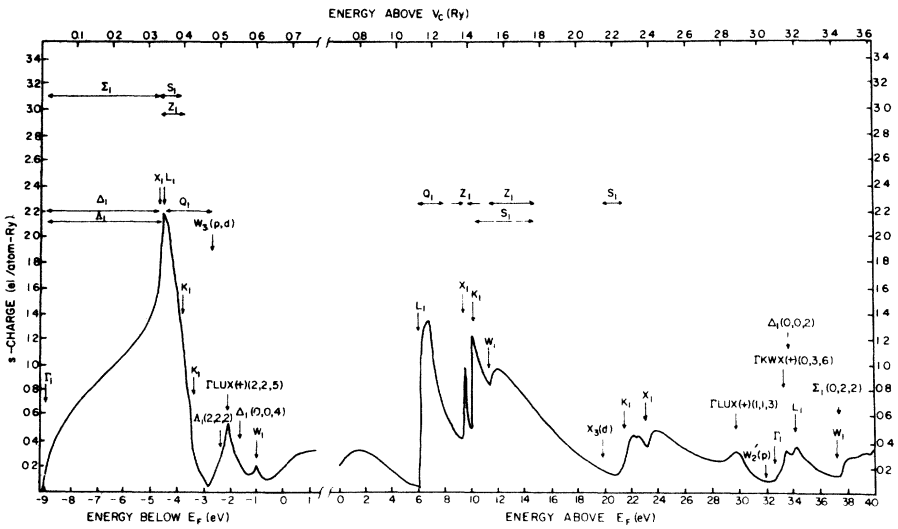

FIG. 3. s partial density of states for Ni.

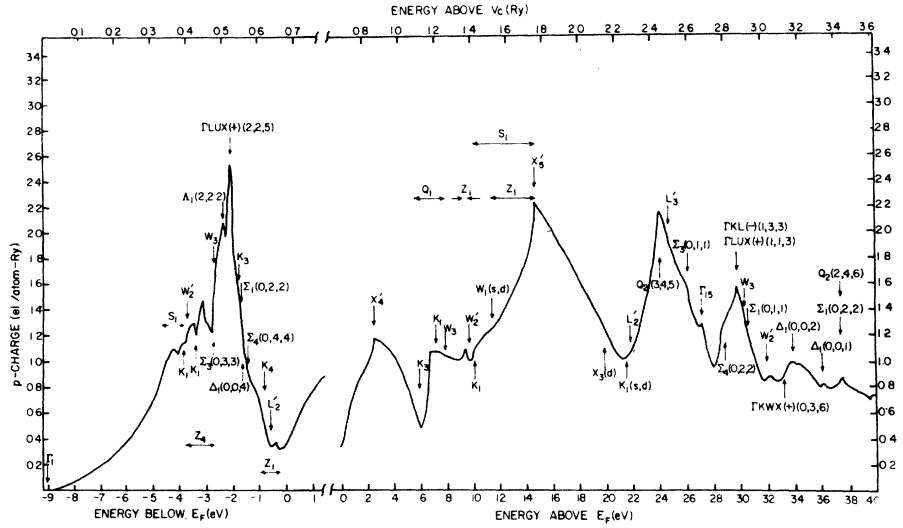

FIG. 4. p partial density of states for Ni.

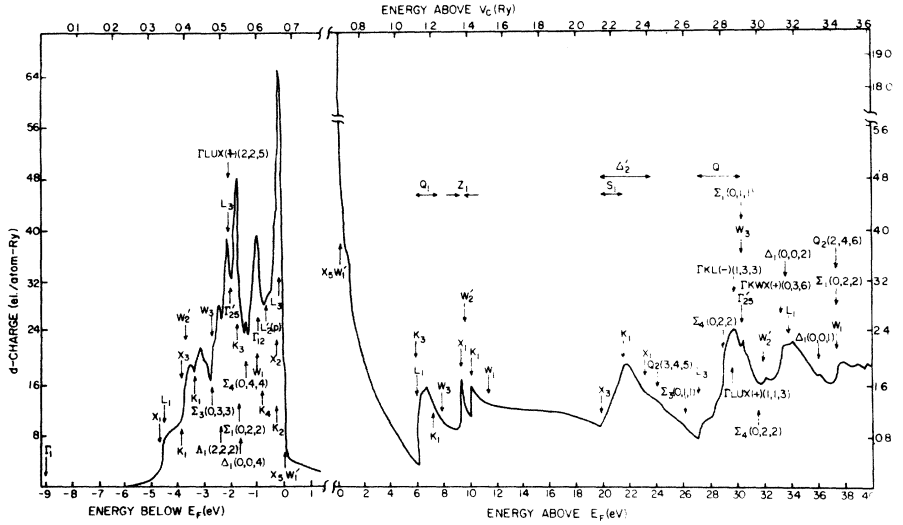

FIG. 5. d partial density of states for Ni.

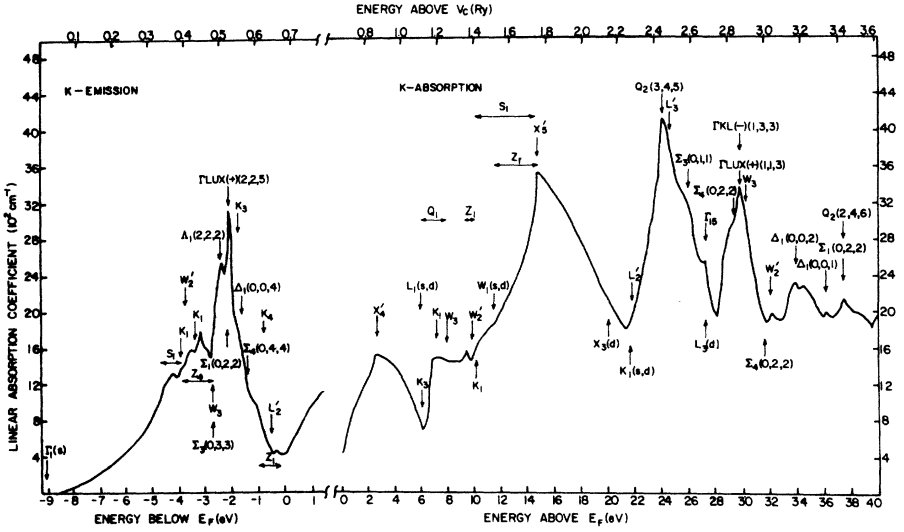

FIG. 6. Computed x-ray K spectrum for Ni. The spectrum below E_F is proportional to the K emission rate.

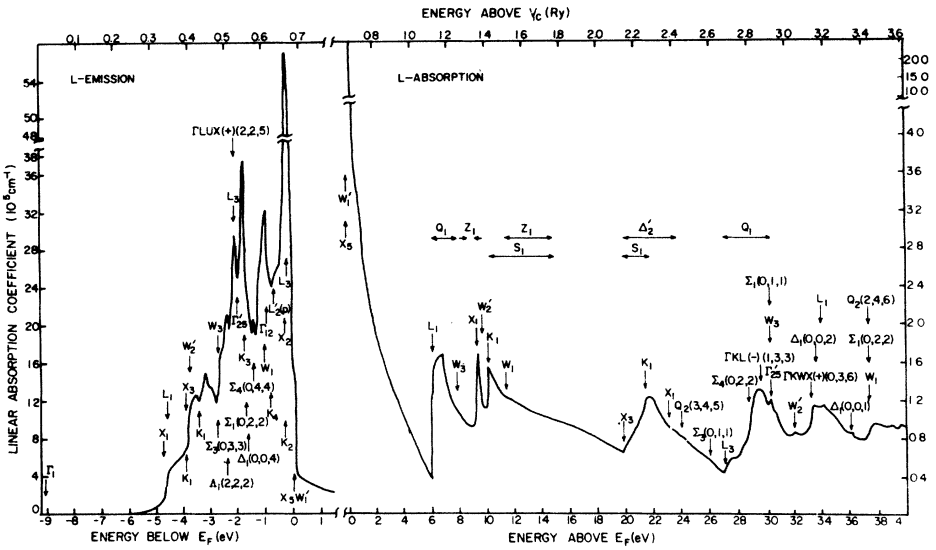

FIG. 7. Computed x-ray L spectrum for Ni.

This last feature was not reported by Papaconstantopoulos *et al.*[5] At higher energies there are peaks at K_1 in the energy region of a flat Δ_2' d band; $\Gamma KL(-)(1,3,3)$; $\Gamma KWX(+)(0,3,6)$, $\Delta_1(0,0,2)$, and L_1; and at W_1.

V. SPECTRUM BROADENING

The calculated spectra should be broadened to account for the finite width of the inner-state core level. Several values have been reported for both K and L_{III} shell widths in nickel; unfortunately, both numbers appear uncertain to at least ±0.1 eV. The resulting uncertainty in the broadening is not particularly serious for the K absorption spectrum or for the K and L emission curves; the experimental and theoretical structures present are sufficiently broad so that uncertainties in the core-hole width will not much influence the trend of our comparisons between theory and experiment. However, for the L_{III} absorption edge the high-spike characteristic of the unfilled $3d$ states near the Fermi edge is so sharp that almost the entire width of the theoretical curve will be due to the inner-state core-level broadening.

Earlier measurements of the core-level widths include those of Beeman and Bearden, who have fit their nickel K absorption edge to the arctangent shape derived by Richtmeyer, Barnes, and Ramberg, and deduced a K-shell broadening of 1.9 ± 0.5 eV.[29] Bonnelle lists values of K- and L-shell widths obtained by various means and infers, in addition to the results of Beeman and Bearden, a value of 1.35 eV for the K shell width of nickel; 0.7, 0.97, and 0.97 eV for the L_{III} width; and 1.7 and 1.49 eV for the L_{II} width.[30] Recent precision measurements of the core line by x-ray photoelectron spectroscopy (XPS) reveal asymmetric $2P_{1/2}$ and $2P_{3/2}$ core levels.[31] When fit to the theory of Donaich and Sunjic, the Lorentzian portion of the curve fit has full widths of 1.6 and 0.94 eV, respectively, for the $2P_{1/2}$ and $2P_{3/2}$ lines. Finally, Suonninen and Valkonnen have done precise measurements on nickel emission lines in pure Ni and Ni-Al alloys and find a full width at half-maximum of the nickel $K\alpha_1$ line of 2.46 eV, which gives a measure of the sum of the K and L_{III} level widths.[32] The core-hole broadening we use for the nickel K edge is 1.8 eV. As mentioned above, the exact choice of the K width value is not particularly crucial. For the L_{III} level width we chose a value of 0.8 eV. This value was chosen to be somewhat to the small side of the average of the various experimental values, for reasons given below. For the L_{II} level width, Bonnelle's table indicates a value ~1.0 eV greater than the L_{III} width; thus we use a L_{II} width of 1.8 eV. The final $L_{III,II}$ theoretical curve is formed by weighting the appropriately broadened L_{III} and L_{II} spectra by the statistical ratio of two to one and summing, assuming a splitting of 17.26 eV as taken from Bearden and Burr.[33]

The exchange splitting in ferromagnetic Ni, estimated to be about 0.35 eV,[34] is small in comparison with the K and L core-level widths. Therefore, the core-level broadened theoretical spectra for paramagnetic Ni should not differ appreciably from those obtained using a ferromagnetic calculation. This insensitivity of x-ray experiments involving deep core levels has been demonstrated by the appearance potential spectroscopy (APS) of Ni by Wandelt *et al.*[35] They observe that the thres-

hold behavior for ionization of the L_{III} shell of Ni by electron impact remains constant with temperature even beyond the Curie point.

VI. EXPERIMENTAL METHODS

The $L_{III,II}$ absorption edge used in our comparisons between theory and experiment is newly measured. Though the K edge has been reported previously,[36] for completeness experimental details are briefly included for it as well as the L absorption spectra. For the K edge, silicon monochromater crystals were used whose first-order rocking curve width is equivalent to a resolution of 0.78 eV at the nickel K edge. A tungsten target x-ray tube was used in conjunction with a beryllium exit window and a sealed-off proportional counter. For the L edge, rubidium acid phthalate (RAP) crystals were used whose first-order rocking curve width was approximately 450 arc secs. This rocking curve width is equivalent to a resolution of 1.4 eV at the nickel L edge. For L edges, we found it advantageous to use a pure copper target on the demountable x-ray tube. A flow proportional counter outfitted with an aluminized polypropelene window was used for x-ray detection, and polypropelene was used as well for the exit window of the x-ray tube. Both L and K edges were measured using a vacuum two-crystal spectrometer described previously.[37] For the K-edge results shown, a 4-μm nickel foil was used for which thickness effects were estimated to be small.[38] For the L edges, varying thicknesses of nickel were evaporated at pressures of $\sim 10^{-5}$ Torr onto stretched polypropelene films which were in contact with a water-cooled copper block. Deposits of nickel film evaporated under the same vacuum conditions as the samples were checked by x-ray diffraction and found to be characteristic of pure nickel. The following additional test of the samples was carried out. Nickel films of the order 0.1-μ thick were evaporated onto sheets of ~2-μ aluminum. The substrate sheets were then cut into strips and many strips sandwiched together to make an effective thickness of about 4 μ of nickel. The aluminum in the resulting sandwich was sufficiently transparent so that K edges of the evaporated nickel could be measured and compared with K edges from rolled or electroplated foils. We found that as long as we evaporated our nickel from tungsten boats which were protected with an Al_2O_3 coating, K edges from rolled and evaporated films were the same

Possible effects of the polypropelene substrate were considered. Tomboulian and Pell reported that a zapon backing had a pronounced effect on the aluminum $L_{2,3}$ edge.[39] However, a more recent measurement by Haensel, Sonntag, Kunz, and Sasaki[40] using zapon-backed aluminum agrees fairly well with the measurements of Gahwiller and Brown[41] using unbacked foils. In addition, we have measured nickel L_{III} edges on backings of carbon as well as polypropelene and found no significant difference in the shape of the nickel edges for the two cases. From all of the above evidence it appears likely that the polypropelene substrates have negligible effects on the spectra.

In recording sharp spectra such as the nickel L_{III} edge, particular attention must be paid to the "thickness effect." Experimentally, it is found that the shape of an absorption edge near the absorption discontinuity is dependent on absorber thickness. The effect was discovered by Parratt, Hempstead, and Jossen.[42] These authors deduced that the long tails of the instrumental window will pass low-energy photons in any measurement taken ostensibly of high-energy x rays. The high-energy x rays are absorbed much more strongly than the x rays of energies less than that of an absorption discontinuity; thus, the relative error introduced into measurements of x-ray energies above an absorption threshold will worsen for thicker foils. Porteus developed a method by which one could deconvolute instrumental errors assuming the instrumental window function is known.[43] However, in practice, thickness effects may not readily be removed by deconvolution, partially because of uncertainties in the knowledge of the tails of the window function.[38] For a simple model of the thickness effect in K edges of nickel, the shape of the normalized experimental absorption edge does approach the true spectrum in the limit of zero-thickness foils, although even in the thin-foil limit there is a small relative error in the low-absorption portion of the edge.[38]

Although the shape of the experimental spectrum approaches most nearly the "true" absorption edge for vanishingly thin foils, the relative *statistical* accuracy of the data will deteriorate, as discussed by Nordfors.[44] Thus, for the $L_{III,II}$ edges of nickel one has competing requirements of optimum thickness, depending on whether one wishes to accurately determine the correct peak-to-valley ratio $R = (A - X)/(C - X)$ in Fig. 8, or one wishes to measure gentle fine structure such as peak C in Fig. 8. R is most accurately determined using the thinnest foils possible, whereas a weak peak such as C does not constitute much of an absorption contrast relative to neighboring portions of the spectra and will not be much affected by sample thickness. Statistical errors are more of an obstacle to observations of peak C than are thickness effects; consequently, measurements on peak C were carried out using thicker samples. We chose

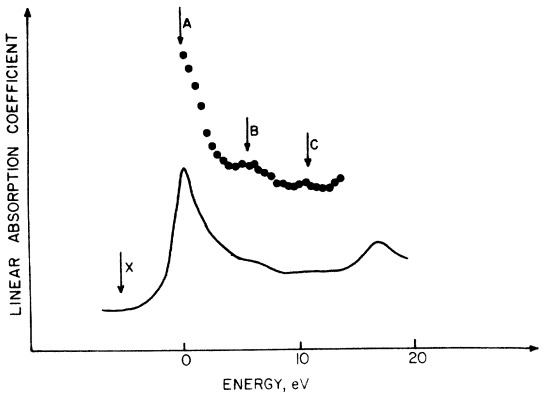

FIG. 8. Experimental $L_{III,\,II}$ edge results without deconvolution. The top curve is the averaged thick-foil spectrum for peaks A, B, and C. The bottom curve is a combination of thick- and thin-foil results constructed as described in the text.

the following procedure. First, nickel L_{III} edges were measured for several thicknesses of foils and a plot made of the quantity $A - X$ vs $C - X$. For foils so thin that thickness effects are absent, such a plot will approach a straight line passing through the origin. Such a plot was made for many foils of differing thicknesses, and the resulting curve indicated that thickness effects are almost but not quite removed for the thinnest foils used. The absorption edges of several such thin foils were measured and their average spectrum used to determine the general shape of the $L_{III,II}$ edge such as the R ratio and the ratio of L_{III} to L_{II} peak heights. The results of the thick-foil measurements are shown in Fig. 8 and show, in addition to peak B, the weak structure at C undetected in previous measurements of Bonnelle.[30] In order to obtain the most accurate experimental curve, a combination of thick- and thin-foil results was made. A spectrum was drawn representing an average of thin-foil results except that a flat line was drawn through the region corresponding to peak C. The thick-foil measurement of peak C was then suitably scaled down and joined to the thin-foil curve. The final thick-thin foil combined spectrum is shown in Fig. 8. Finally, in order to correct for the central portion of the instrumental window, the data of Fig. 8 was deconvoluted with a Lorentzian approximation to the rocking curve, using the method of Schnopper.[45]

It is of interest to compare the resulting $L_{III,II}$ edges with previous experimental results. Bonnelle shows several sets of nickel curves. In one set of spectra, only the L_{III} edge is measured for several thicknesses, and a pronounced thickness effect is apparent, in agreement with present results. The thinnest foil measured has an R value of about 4.4. However, taking into account all experimental considerations, including insuring linear detection for the photographic registration method used, Bonnelle obtains a curve which she feels approaches closest to the correct spectrum which as an R value of about 4.0, in approximate agreement with our average R value. In the spectrum obtained by Bonnelle showing both L_{III} and L_{II} peaks, the R value appears to be about 3.6. Thus, Bonnelle's curve showing both L_{III} and L_{II} peaks probably corresponds to a foil somewhat thicker than optimum. The latter spectrum was used by Nagel and Papaconstantopoulos to compare to their theoretical calculations.[5] As indicated here, the experimental curve used for this comparison had an R value which was too small. As thickness effects are removed, the ratio of L_{III} to L_{II} peak heights will increase markedly. Thus, in Bonnelle's combined $L_{III,II}$ spectrum, for which the R value indicates a somewhat thick foil, the L_{II} peak height is about 0.6 the L_{III} height, whereas our results show the ratio of L_{III} to L_{II} heights to be greater than two to one. Upon deconvolution, the ratio of L_{III} to L_{II} heights increases still further.

In regard to peak C, it is of interest to consider some old results on the nickel $L_{III,II}$ edge obtained by Van den Berg, in which a nickel $L_{III,II}$ edge was obtained whose L_{II} height was greater than the L_{III} height, indicating a very large thickness effect.[46,47] For thick samples, peak C should show up quite clearly and indeed Van den Berg does obtain two peaks between the L_{III} and L_{II} maxima corresponding roughly to our peaks B and C. Finally, Liefeld has obtained a nickel L absorption curve from a self-absorption correction to an L valence emission spectrum.[48] This self-absorption correction has the appearance of a thickness-effect–distorted-absorption edge containing both peaks B and C. In summing up, it appears that our nickel $L_{III,II}$ edge contains some features in common with all previous results, but it is the first to combine all the spectral features into one curve for which corrections are made for effects of the instrumental window.

VII. COMPARISON BETWEEN THEORY AND EXPERIMENT

We consider first the K absorption edge. The theoretical curve is displayed adjacent to the deconvoluted experimental spectrum in Fig. 9. The vertical scales for the two curves are plotted in terms of actually calculated theoretical values and measured experimental absorption coefficients so that there are no adjustments of the heights of either curves. Because the Fermi energy of the experimental curve is not known absolutely, the first inflection points of the theoretical and experi-

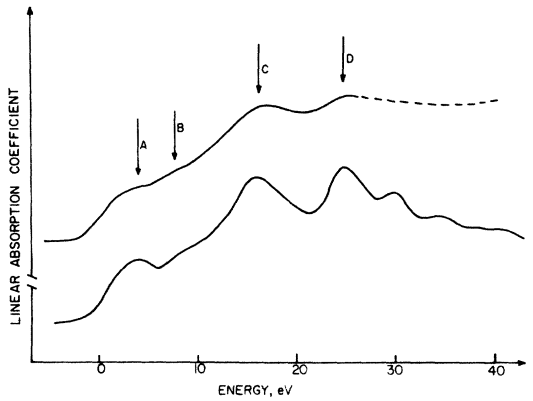

FIG. 9. Comparison between experimental and theoretical K edges. From top to bottom are the nickel K edge corrected for instrumental distortion and the broadened theoretical K edge. The dashed lines are experimental points taken on an older spectrometer.

mental curves are approximately lined up. There is no other adjustable parametrization or tilting. We discuss the theoretical-experimental comparison in three main regions separately. Above about 25 eV, the average height of the theoretical curve drops relative to that of the experimental spectrum. At least part of this discrepancy is due to the fact that band structure at energies higher than 40 eV or so, which of necessity is not included in the calculation, contributes to regions below 40 eV of the experimental curve as the result of the hot-electron broadening. From about 6 to 25 eV, the comparison between theory and experiment is excellent. The gentle shoulder positioned at peak B agrees almost exactly with experiment, in contrast to the results of previous calculations. Peaks C and D are sharper in the theoretical curve, which is to be expected because of the effects of hot-electron broadening. Turning now to the region from threshold to about 6 eV, we see that although the calculation agrees qualitatively with the experiment, there is a definite rounding of the experimental curve relative to the calculation. We consider possible broadening mechanisms to account for the discrepancy. Hot-electron broadening must approach zero at the Fermi level and cannot account for the difference.[5] Flynn has estimated phonon-broadening widths for core-level excitations in many materials.[49] The estimated phonon-broadening width for nickel is far too small to account for the difference between experimental and theoretical curves near threshold. We conclude, then, that a careful one-electron band calculation, neglecting effects of the core hole on the crystal, yields excellent agreement with the observed nickel K edge except near threshold where the experimental spectrum is without doubt somewhat rounded relative to the one-electron crystal calculation.

We consider next the $L_{\mathrm{III,II}}$ absorption spectrum, Fig. 10. For the experimental curves the thickness of the samples are not accurately known, so the experimental and theoretical curves are normalized on the vertical scale such that the centroid of the experimental and theoretical peaks C coincide. Again, general agreement between theory and experiment is good. Within experimental error, our $L_{\mathrm{III,II}}$ peak separation agrees with the value obtained from Bearden and Burr.[33] Peak C lines up well between experiment and theory. Regarding the main absorption peak at A, it is unfortunate, as discussed above, that the width of the inner-state core level is not better known. The broadening chosen, however, of 0.8 eV is on the narrow side of the majority of the experimental results for the $2P_{3/2}$ core width. Thus, the resulting theoretical curve is probably slightly underbroadened. Despite this fact, the main edge at A in the L spectrum is the only structure, for both K or L absorption spectra, where the experimental spectrum is sharper than the theoretical curve. Finally, we note that the experimental spectrum does not show the large dip preceding peak B. It is probable that the discrepancies between experiment and theory in the vicinity of peak B would be lessened if one assumed a core level having a skewed shape similar to that measured by XPS.[31]

There is a discrepancy between theory and experiment near threshold. In this regard we mention the Mahan–Nozieres–DeDominicis (MND) theory, as reviewed by Mahan.[50] The theory has so far only been applied to light metals where it predicts an enhanced peaking of L edges and a rounding of K edges at threshold. In addition, there is controversy over the MND theory, it being

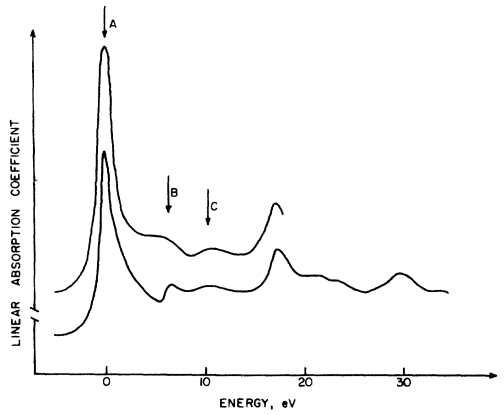

FIG. 10. Comparison between experimental and theoretical $L_{\mathrm{III,\,II}}$ edges. From top to bottom are the nickel L edge corrected for instrumental distortion and the broadened theoretical L edge.

supported by the results of Citrin *et al.*,[51] and disputed by Dow, Watson, and Fabian who contend that the MND theory really predicts K edges are enhanced rather than rounded in the case of simple metals.[52] Without entering into the controversy, we find that at threshold, the experimental K edge of nickel is without doubt rounded relative to the results of a one-electron crystal calculation. There is somewhat less certainty in the case of the L edge because of the sensitivity of the theoretical results to the width and shape of the $2P_{3/2}$ core-hole level; however, we find that in contrast to the case of the K edge, the experimental L edge of nickel is almost certainly enhanced relative to the theoretical curve.

We consider next the comparison between the present calculations for emission spectra and the experimental results existing in the literature. For the L emission spectra there exists considerable discrepancy between the various experimental results. Bonnelle, using a bent crystal and 2500-V excitation at a pressure of 10^{-5} Torr found a considerable portion of the emission curve above the Fermi level.[30] Chopra and Liefeld showed that there was a self-absorption distortion in the spectrum unless one went to low-excitation voltages.[48,53] They found that a structure they attributed to high-energy satellites persisted unless they lowered their excitation voltage to a value less than that necessary to excite the L_{II} core level. Hanzely and Liefeld corrected for self-absorption and satellite emission in a similar manner but still found significant area under the emission curve persisting above the Fermi level, which they associated with a possible bound-ejected-electron (BEE) state.[54,55] Hanzely's work, as well as that of Chopra and Liefeld, was done at pressures of 10^{-9} Torr using a two-crystal spectrometer with measured resolutions of 0.65 eV. Holliday repeated the work of Liefeld and Chopra, using a blazed-grating spectrometer and a special tube designed to minimize self-absorption.[56] Holliday obtained a broad emission spectrum which showed no evidences of self-absorption or satellite reduction with changes in excitation voltage. He suggested that the self-absorption results of Chopra and Liefeld might be due to sample contamination. With respect to this point, we feel that Chopra and Liefeld were certainly making a genuine self-absorption correction since the resulting self-absorption curve contains all of the essential structure of the nickel L absorption edge. Willens and Brasen measured the L emission spectrum using a bent potassium acid phthalate (KAP) crystal.[57] Their spectrum has almost half the emission band above the position of the absorption-edge white line. In the main thrust of their work, Willens and Brasen obtained modulated nickel spectra using an alternating mechanical strain, to record the piezo soft x-ray spectrum. The results depended upon amount of previous cold working of the sample, and whether or not it was annealed. The authors find modulation structures at about 5.5 eV above the main peak and a low-energy structure about 5 to 6 eV below the Fermi level. They suggest that the high-energy structure is associated with an asymmetric inner-state core level, rather than satellite structure, and that the low-energy peak is truly a band-structure feature. Finally, Dev and Brinkman's L spectrum, measured with a plane mica crystal, has a full width of only 1.6 eV after corrections were made for instrumental broadening and the inner-level width.[58] These authors contend that the emission spectrum has a width very much less than the conduction band, and that emission spectra, as opposed to absorption spectra, are characteristic of localized states of the metal ion.

The absorption edges, which are obtained by measurements on a bulk sample and are free of the complexities of possible satellite emissions, furnish a better vehicle for comparison to band-structure theories than do the emission curves. The variation between experimental emission spectra is so great that it is difficult to make a meaningful comparison between theory and experiment. The spectrum of Hanzely and Liefeld is shown in comparison with theory in Fig. 11. Most of the emission spectra taken do seem to be narrower than the calculated spectrum. We note that the valence-band electron spectroscopy for chemical analysis (ESCA) spectrum for nickel is found to be narrower than expected, as well.[59] Of all the emission spectra, the one which agrees best with our calculated L_{III} spectrum is the M_{III} $(3P_{3/2})$ emission band measured by Cuthill *et al.*[60] (Fig. 11). This

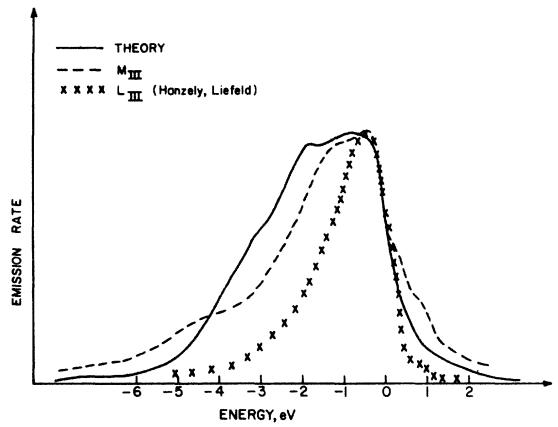

FIG. 11. Experimental and theoretical L emission spectra. The Fermi levels are lines up at zero on the horizontal scale.

spectrum is presented on the same graph only because it shows a double hump similar to that in the calculated L_{III} curve. Finally, we consider the calculated K emission spectrum. The most recent K valence-band emission-spectrum measurement of which we are aware is that of Nemoshkalenko *et al.*,[61] where agreement between experiment and theory is poor, and there is clearly a need for further experimental work on the K valence-band spectrum of nickel.

VIII. CONCLUSIONS

The present study compares with experiment a detailed one-electron calculation of x-ray spectra, with the inclusion of the transition probabilities. The comparison is difficult in the case of emission spectra because of complicating effects in the interpretation of the experimental results, although most of the experimental x-ray valence-band spectra are much narrower than our calculated L spectrum. For absorption spectra, theoretical and experimental results are generally in excellent agreement.

ACKNOWLEDGMENTS

We are grateful for stimulating discussions with Drs. L. V. Azaroff and P. E. Best. We are indebted to Steve Kao for assistance with sample preparation. We are especially grateful to Mike Varanka for much dedicated and invaluable work on the automation aspects of the spectrometer. This research was supported in part by grants from the NSF and from the U. S. Army Research Office.

[1]A. B. Chen and B. Segall, Phys. Rev. B 12, 600 (1975).
[2]F. Szmulowicz, Ph.D. thesis (CWRU Cleveland, Ohio, 1977) (unpublished); F. Szmulowicz and B. Segall, *International Conference on the Physics of X-Ray Spectra* (Natl. Bur. Stand., Gaithsburg, Md., 1976), p. 202.
[3]R. P. Gupta and A. J. Freeman, Phys. Rev. Lett. 36, 1194 (1976).
[4]J. W. McCaffrey and D. A. Papaconstantopoulos, Solid State Commun. 14, 1055 (1974).
[5]D. J. Nagel, D. A. Papaconstantopoulos, J. W. McCaffrey, and J. W. Criss, *Proceedings of the International Symposium on X-Ray Spectra and Electronic Structure of Matter*, edited by A. Faessler and G. Wiech (Academic, New York, 1973), p. 51; D. J. Nagel, in *Band Structure Spectroscopy of Metals and Alloys*, edited by D. J. Fabian and L. M. Watson (Academic, New York, 1973), pp. 457–489.
[6]D. A. Papaconstantopoulos, Phys. Rev. Lett. 31, 1050 (1973).
[7]D. A. Papaconstantopoulos, *International Conference on the Physics of X-Ray Spectra* (Natl. Bur. Stand., Gaithsburg, Md., 1976), p. 192.
[8]G. Gilat and L. J. Raubenheimer, Phys. Rev. 144, 390 (1966).
[9]G. M. Stocks, R. W. Williams, and J. S. Faulkner, Phys. Rev. B 4, 4390 (1971).
[10]J. G. Hanus, MIT Solid State and Molecular Theory Group Quarterly Progr. Rep. No. 44, 29 (1962) (unpublished).
[11]J. Yamashita, M. Fukuchi, and S. Wakoh, J. Phys. Soc. Jpn. 18, 999 (1963).
[12]S. Wakoh and J. Yamashita, J. Phys. Soc. Jpn. 19, 1342 (1964).
[13]S. Wakoh, J. Phys. Soc. Jpn. 20, 1894 (1965).
[14]E. C. Snow, J. T. Waber, and A. C. Switendick, J. Appl. Phys. 37, 1342 (1966).
[15]J. W. D. Connolly, Phys. Rev. 159, 415 (1967).
[16]L. Hodges, H. Ehrenreich, and N. D. Lang, Phys. Rev. 152, 505 (1966).
[17]H. Ehrenreich, H. R. Philipp, and D. J. Olechna, Phys. Rev. 131, 2469 (1963).
[18]F. M. Mueller, Nat. Bur. Stand., (U.S.) Spec Publ. No. 323, edited by L. H. Bennett (U.S. GPO, Washington, D. C., 1964), p. 17.
[19]J. Langlinais and J. Callaway, Phys. Rev. B 5, 124 (1972).
[20]J. Callaway and C. S. Wang, Phys. Rev. B 7, 1096 (1973).
[21]C. S. Wang and J. Callaway, Phys. Rev. B 9, 4897 (1974).
[22]C. S. Wang and J. Callaway, Phys. Rev. B 15, 298 (1977).
[23]V. L. Moruzzi, A. R. Williams, and J. F. Janak (unpublished).
[24]L. F. Mattheiss, J. H. Wood, and A. C. Switendick, *Methods in Computational Physics*, edited by B. Alder, S. Fernbach, and M. Rotenberg (Academic, New York, 1968), Vol. 8, pp. 110–111.
[25]F. Herman and S. Skillman, *Atomic Structure Calculations* (Prentice-Hall, Englewood Cliffs, N.J., 1963).
[26]L. F. Mattheiss, Phys. Rev. 133, A1399 (1964); 134, A970 (1964).
[27]G. A. Burdick,, Phys. Rev. 129, 138 (1963).
[28]J. F. Janak, A. R. Williams, and V. L. Moruzzi, Phys. Rev. B 11, 1522 (1975).
[29]W. W. Beeman and H. Friedman, Phys. Rev. 56, 392 (1939).
[30]C. Bonnelle, Ann. Phys. (Paris) I, 439 (1966).
[31]S. Hüfner and G. K. Wertheim, Phys. Lett. 51A, 301 (1975).
[32]E. J. Suoninen and T. V. O. Valkonen, J. Phys. F 5, 837 (1975).
[33]J. A. Bearden and A. F. Burr, Rev. Mod. Phys. 39, 78 (1967).
[34]E. P. Wohlfarth, in *Proceedings of the International Conference on Magnetism, Nottingham, England, 1964* (The Institute of Physics and the Physical Society, London, England, 1965), p. 81.
[35]K. Wandelt, G. Ertl, H. C. Siegmann, and P. S. Bagus, Solid State Commun. 22, 59 (1977).
[36]D. M. Pease and T. K. Gregory, Solid State Commun. 18, 1133 (1976).
[37]T. K. Gregory and P. E. Best, Adv. X-ray Anal. 15, 90 (1971).

[38]D. M. Pease, Appl. Spectrosc. 30, 405 (1976).
[39]D. H. Tomboulian and E. M. Pell, Phys. Rev. 15, 1196 (1951).
[40]R. Haensel, B. Sonntag, C. Kunz, and T. Sasaki, Appl. Phys. 40, 3046 (1969).
[41]C. Gähwiller and F. C. Brown, Phys. Rev. B 2, 1918 (1970).
[42]L. G. Parratt, C. F. Hempstead, and E. L. Jossen, Phys. Rev. 105, 1228 (1957).
[43]J. O. Porteus, J. Appl. Phys. 33, 700 (1962).
[44]B. Nordfors, Ark. Fys. 18, 37 (1960).
[45]H. Schnopper, Ph.D. dissertation (Cornell University, 1962) (unpublished).
[46]L. G. Parratt, Rev. Mod. Phys. 31, 616 (1959).
[47]C. Van der Berg, Ph.D. dissertation (Gröningen University, 1957) (unpublished).
[48]R. J. Liefeld, in *Soft X-Ray Band Spectra*, edited by Derek J. Fabian (Academic, London, 1968).
[49]C. P. Flynn, Phys. Rev. Lett. 37, 1445 (1976).
[50]G. D. Mahan, Solid State Phys. 29, 75 (1974).
[51]P. H. Citrin, G. K. Wertheim, M. Schlüter, and Y. Baer, in *International Conference on the Physics of X-Ray Spectra* (Extended Abstracts) (1976).
[52]J. D. Dow, L. N. Watson, and D. J. Fabian, J. Phys. F 4, L76 (1974).
[53]D. Chopra and R. Liefeld, Bull. Am. Phys. Soc. B 63, 404 (1964).
[54]S. Hanzely and R. J. Liefeld, Natl. Bur. Stand. (U.S.) Publ. No. 323 (U.S. GPO, Washington, D.C., 1971), p. 319.
[55]S. Hanzely, Ph.D. dissertation (New Mexico State University, 1968) (unpublished).
[56]J. E. Holliday, in *Soft X-Ray Band Spectra*, edited by Derek J. Fabian (Academic, London, 1968).
[57]R. H. Willens and D. Brasen, Phys. Rev. B 5, 1891 (1972).
[58]Brahm Dev and H. Brinkman, Physica (Utr.) 57, 616 (1972).
[59]S. Hüfner, G. K. Wertheim, and J. H. Wernick, Phys. Rev. B 8, 4511 (1973).
[60]J. R. Cuthill, A. J. McAlister, M. L. Williams, and R. C. Dobbyn, in *Soft X-Ray Band Spectra*, edited by Derek J. Fabian (Academic, London, 1968).
[61]V. V. Nemoshkalenko, V. V. Gorskiy, and R. F. Korkishko, Phys. Met. Metallogr. (USSR) 31, 193 (1971).